PTEP

Prog. Theor. Exp. Phys. **2013**, 113D02 (17 pages)
DOI: 10.1093/ptep/ptt091

Spin–isospin response of deformed neutron-rich nuclei in a self-consistent Skyrme energy-density-functional approach

Kenichi Yoshida*

Graduate School of Science and Technology, Niigata University, Niigata 950-2181, Japan
*E-mail: kyoshida@nt.sc.niigata-u.ac.jp

Received August 2, 2013; Revised September 5, 2013; Accepted September 30, 2013; Published November 1, 2013

We develop a new framework for the self-consistent deformed proton–neutron quasiparticle-random-phase approximation (pnQRPA), formulated in the Hartree–Fock–Bogoliubov (HFB) single-quasiparticle basis. The same Skyrme force is used in both the HFB and pnQRPA calculations, except in the proton–neutron particle–particle channel, where an $S = 1$ contact force is employed. A numerical application is performed for Gamow–Teller (GT) strength distributions and β-decay rates in the deformed neutron-rich Zr isotopes located around the path of rapid-neutron-capture-process nucleosynthesis. It is found that the GT strength distributions are fragmented due to deformation. Furthermore, we find that the momentum-dependent terms in the particle–hole residual interaction lead to a stronger collectivity of the GT giant resonance. The $T = 0$ pairing enhances the low-lying strengths cooperatively with the $T = 1$ pairing correlation, which shortens the β-decay half-lives by at most an order of magnitude. The new calculation scheme reproduces well the observed isotopic dependence of the β-decay half-lives of deformed $^{100-110}$Zr isotopes.

Subject Index D11, D13

1. Introduction

The study of unstable nuclei has been a major subject in nuclear physics for a couple of decades. The collective mode of excitation emerging in the response of the nucleus to an external field is a manifestation of the interaction among nucleons. Thus, the spin–isospin channel of the interaction and the spin–isospin part of the energy-density functional (EDF), which is crucial for understanding and predicting the properties of unstable nuclei and asymmetric nuclear matter, have been much studied, especially through Gamow–Teller (GT) strength distributions [1,2].

The GT strength distribution has been extensively investigated experimentally and theoretically not only because of interest in nuclear structure but also because β-decay half-lives set a time scale for the rapid-neutron-capture process (r-process), and hence determine the production of heavy elements in the universe [3]. The r-process path is far away from the stability line, and involves neutron-rich nuclei. They are weakly bound and many of them are expected to be deformed according to the systematic Skyrme-EDF calculation [4].

Collective modes of spin–isospin excitation in nuclei are described microscopically by the proton–neutron random-phase approximation (pnRPA) or the proton–neutron quasiparticle-RPA (pnQRPA) including the pairing correlations on top of the self-consistent Hartree–Fock (HF) or HF–Bogoliubov (HFB) mean fields employing the nuclear EDF. There have been many attempts to investigate the

spin–isospin modes of excitation in stable and unstable nuclei [5]. These studies are largely restricted to spherical systems, and the collective modes in deformed nuclei remain mostly unexplored.

The spin–isospin responses of deformed nuclei have been extensively investigated by the Madrid group [6–8] in connection with the studies of beta decay and double-beta decay in a Skyrme–pnQRPA model. The method employed in these preceding works relies on the BCS pairing instead of the HFB pairing, and the residual interactions are treated in a separable approximation. The BCS approximation for pairing is inappropriate for describing weakly bound nuclei due to the unphysical nucleon gas problem [9]. Furthermore, collectivity and details of the strength distribution are sensitive to both the shell structure around the Fermi levels and the residual interactions. Quite recently, in Ref. [10], the fully self-consistent Skyrme–pnQRPA model was established in an HFB single-canonical basis and was applied to the study of double-beta decay.

Recently, β-decay half-lives of neutron-rich Kr to Tc isotopes with $A \simeq 110$ located on the boundary of the r-process path were newly measured at RIKEN RIBF [11]. The ground-state properties such as deformation and superfluidity in neutron-rich Zr isotopes up to the drip line have been studied by employing the Skyrme–HFB method, and it has been predicted that Zr isotopes around $A = 110$ are well deformed in the ground states [12].

In the present article, to investigate the Gamow–Teller mode of excitation and β-decay properties in the deformed neutron-rich Zr isotopes, we construct a new framework of the calculation scheme employing the Skyrme EDF self-consistently in both the static and dynamic levels. Furthermore, to describe properly the pairing correlations in weakly bound systems and coupling to the continuum states, the HFB equations are solved in real space. This framework is extended based on the deformed like-particle QRPA method developed in Ref. [13].

The article is organized as follows: In Sect. 2, the deformed Skyrme–HFB + pnQRPA method for describing the spin–isospin responses is explained. In Sect. 3, the results of the numerical analysis of the giant resonance in neutron-rich Zr isotopes are presented. A discussion on the effects of the $T = 0$ pairing is included. Finally, a summary is given in Sect. 4.

2. Theoretical framework

2.1. *Microscopic calculation of spin–isospin modes of excitation in deformed nuclei*

To describe the nuclear deformation and the pairing correlations in the ground state simultaneously, taking the continuum into account properly, we solve the HFB equations [9,14]

$$\begin{pmatrix} h^q(\boldsymbol{r}\sigma) - \lambda^q & \tilde{h}^q(\boldsymbol{r}\sigma) \\ \tilde{h}^q(\boldsymbol{r}\sigma) & -(h^q(\boldsymbol{r}\sigma) - \lambda^q) \end{pmatrix} \begin{pmatrix} \varphi^q_{1,\alpha}(\boldsymbol{r}\sigma) \\ \varphi^q_{2,\alpha}(\boldsymbol{r}\sigma) \end{pmatrix} = E_\alpha \begin{pmatrix} \varphi^q_{1,\alpha}(\boldsymbol{r}\sigma) \\ \varphi^q_{2,\alpha}(\boldsymbol{r}\sigma) \end{pmatrix} \tag{1}$$

in coordinate space using cylindrical coordinates $\boldsymbol{r} = (\rho, z, \phi)$. We assume axial and reflection symmetries. Here, the superscript q denotes ν (neutron, $t_z = 1/2$) or π (proton, $t_z = -1/2$). The mean-field Hamiltonian h is derived from the Skyrme EDF. The pairing field $\tilde{h}$ is treated by using the density-dependent contact interaction [15],

$$v_{\rm pair}(\boldsymbol{r}\sigma, \boldsymbol{r}'\sigma') = \frac{1 - P_\sigma}{2} \left[t'_0 + \frac{t'_3}{6} \varrho_0(\boldsymbol{r}) \right] \delta(\boldsymbol{r} - \boldsymbol{r}'), \tag{2}$$

where $\varrho_0(\boldsymbol{r})$ denotes the isoscalar density and P_σ the spin exchange operator.

Since we consider even–even mother (target) nuclei only, the time-reversal symmetry is assumed. A nucleon creation operator $\hat{\psi}^\dagger_q(\boldsymbol{r}\sigma)$ at the position $\boldsymbol{r}$ with the intrinsic spin σ is then written in terms

of the quasiparticle (qp) wave functions as

$$\hat{\psi}_q^\dagger(\boldsymbol{r}\sigma) = \sum_\alpha \varphi_{1,\alpha}^q(\boldsymbol{r}\bar{\sigma})\hat{a}_{\alpha,q}^\dagger + \varphi_{2,\alpha}^{q*}(\boldsymbol{r}\sigma)\hat{a}_{\alpha,q}. \tag{3}$$

The notation $\varphi(\boldsymbol{r}\bar{\sigma})$ is defined by $\varphi(\boldsymbol{r}\bar{\sigma}) = -2\sigma\varphi(\boldsymbol{r}-\sigma)$.

Using the quasiparticle basis obtained as a self-consistent solution of the HFB equations (1), we solve the pnQRPA equation

$$[\hat{H}', \hat{O}_i^\dagger]|0\rangle = \omega_i \hat{O}_i^\dagger|0\rangle, \tag{4}$$

with $\hat{H}' = \hat{H} - \lambda_\nu \hat{N}_\nu - \lambda_\pi \hat{N}_\pi$. The charge-changing QRPA phonon operators are defined as

$$\hat{O}_i^\dagger = \sum_{\alpha\beta} X_{\alpha\beta}^i \hat{a}_{\alpha,\nu}^\dagger \hat{a}_{\beta,\pi}^\dagger - Y_{\alpha\beta}^i \hat{a}_{\bar{\beta},\pi}\hat{a}_{\bar{\alpha},\nu}, \tag{5}$$

where $\hat{a}_{\bar{\alpha},q}$ is a quasiparticle annihilation operator of the time-reversed state of α.

In the present calculation, we solve the pnQRPA equation (4) in the matrix formulation

$$\sum_{\alpha'\beta'} \begin{pmatrix} A_{\alpha\beta\alpha'\beta'} & B_{\alpha\beta\alpha'\beta'} \\ B^*_{\alpha\beta\alpha'\beta'} & A^*_{\alpha\beta\alpha'\beta'} \end{pmatrix} \begin{pmatrix} X^i_{\alpha'\beta'} \\ Y^i_{\alpha'\beta'} \end{pmatrix} = \omega_i \begin{pmatrix} 1 & 0 \\ 0 & -1 \end{pmatrix} \begin{pmatrix} X^i_{\alpha\beta} \\ Y^i_{\alpha\beta} \end{pmatrix}. \tag{6}$$

Using the qp wave functions $\varphi_1(\boldsymbol{r}\sigma)$ and $\varphi_2(\boldsymbol{r}\sigma)$, the solutions of the coordinate-space HFB equation (1), the matrix elements of (6) are written as

$$\begin{aligned}
A_{\alpha\beta\alpha'\beta'} &= (E_\alpha + E_\beta)\delta_{\alpha\alpha'}\delta_{\beta\beta'} \\
&\quad + \int d1d2d1'd2'\{\varphi_{1,\alpha}^\nu(\boldsymbol{r}_1\bar{\sigma}_1)\varphi_{1,\beta}^\pi(\boldsymbol{r}_2\bar{\sigma}_2)\bar{v}_{\rm pp}(12;1'2')\varphi_{1,\alpha'}^{\nu*}(\boldsymbol{r}'_1\bar{\sigma}'_1)\varphi_{1,\beta'}^{\pi*}(\boldsymbol{r}'_2\bar{\sigma}'_2) \\
&\quad + \varphi_{2,\alpha}^\nu(\boldsymbol{r}_1\sigma_1)\varphi_{2,\beta}^\pi(\boldsymbol{r}_2\sigma_2)\bar{v}_{\rm pp}(12;1'2')\varphi_{2,\alpha'}^{\nu*}(\boldsymbol{r}'_1\sigma'_1)\varphi_{2,\beta'}^{\pi*}(\boldsymbol{r}'_2\sigma'_2) \\
&\quad + \varphi_{1,\alpha}^\nu(\boldsymbol{r}_1\bar{\sigma}_1)\varphi_{2,\beta'}^{\pi*}(\boldsymbol{r}_2\sigma_2)\bar{v}_{\rm ph}(12;1'2')\varphi_{2,\beta}^\pi(\boldsymbol{r}'_1\sigma'_1)\varphi_{1,\alpha'}^{\nu*}(\boldsymbol{r}'_2\bar{\sigma}'_2) \\
&\quad + \varphi_{1,\beta}^\pi(\boldsymbol{r}_1\bar{\sigma}_1)\varphi_{2,\alpha'}^{\nu*}(\boldsymbol{r}_2\sigma_2)\bar{v}_{\rm ph}(12;1'2')\varphi_{2,\alpha}^\nu(\boldsymbol{r}'_1\sigma'_1)\varphi_{1,\beta'}^{\pi*}(\boldsymbol{r}'_2\bar{\sigma}'_2)\}, \qquad (7) \\
B_{\alpha\beta\alpha'\beta'} &= \int d1d2d1'd2'\{-\varphi_{1,\alpha}^\nu(\boldsymbol{r}_1\bar{\sigma}_1)\varphi_{1,\beta}^\pi(\boldsymbol{r}_2\bar{\sigma}_2)\bar{v}_{\rm pp}(12;1'2')\varphi_{2,\bar{\alpha}'}^\nu(\boldsymbol{r}'_1\sigma'_1)\varphi_{2,\bar{\beta}'}^\pi(\boldsymbol{r}'_2\sigma'_2) \\
&\quad - \varphi_{2,\alpha}^\nu(\boldsymbol{r}_1\sigma_1)\varphi_{2,\beta}^\pi(\boldsymbol{r}_2\sigma_2)\bar{v}_{\rm pp}(12;1'2')\varphi_{1,\bar{\alpha}'}^\nu(\boldsymbol{r}'_1\bar{\sigma}'_1)\varphi_{1,\bar{\beta}'}^\pi(\boldsymbol{r}'_2\bar{\sigma}'_2) \\
&\quad - \varphi_{1,\alpha}^\nu(\boldsymbol{r}_1\bar{\sigma}_1)\varphi_{1,\bar{\beta}'}^\pi(\boldsymbol{r}_2\bar{\sigma}_2)\bar{v}_{\rm ph}(12;1'2')\varphi_{2,\beta}^\pi(\boldsymbol{r}'_1\sigma'_1)\varphi_{2,\bar{\alpha}'}^\nu(\boldsymbol{r}'_2\sigma'_2) \\
&\quad - \varphi_{1,\beta}^\pi(\boldsymbol{r}_1\bar{\sigma}_1)\varphi_{1,\bar{\alpha}'}^\nu(\boldsymbol{r}_2\bar{\sigma}_2)\bar{v}_{\rm ph}(12;1'2')\varphi_{2,\alpha}^\nu(\boldsymbol{r}'_1\sigma'_1)\varphi_{2,\bar{\beta}'}^\pi(\boldsymbol{r}'_2\sigma'_2)\}. \qquad (8)
\end{aligned}$$

Here, the time-reversed state is defined as

$$\varphi_{\bar{i}}(\boldsymbol{r}\sigma) = -2\sigma\varphi_i^*(\boldsymbol{r}-\sigma), \tag{9}$$

and $\int d1$ stands for $\sum_{\sigma_1}\int d\boldsymbol{r}_1$.

If one assumes that the effective interaction in the particle–hole (p–h) channel is local, $\bar{v}_{\rm ph}$ is written as

$$\bar{v}_{\rm ph}(12;1'2') = V_{\rm ph}(\boldsymbol{r}_1\sigma_1\tau_1, \boldsymbol{r}_2\sigma_2\tau_2)\delta(\boldsymbol{r}'_1 - \boldsymbol{r}_1)\delta_{\sigma'_1,\sigma_1}\delta_{\tau'_1,\tau_1}\delta(\boldsymbol{r}'_2 - \boldsymbol{r}_2)\delta_{\sigma'_2,\sigma_2}\delta_{\tau'_2,\tau_2}, \tag{10}$$

and $V_{\rm ph}$ is derived from the Skyrme EDF as

$$\begin{aligned} V_{\rm ph}(\boldsymbol{r}_1\sigma_1\tau_1, \boldsymbol{r}_2\sigma_2\tau_2) = {} & [v_{00}(\boldsymbol{r}_1) + v_{01}(\boldsymbol{r}_1)\sigma_1\cdot\sigma_2]\tau_1\cdot\tau_2\delta(\boldsymbol{r}_1 - \boldsymbol{r}_2) \\ & + (v_{10} + v_{11}\sigma_1\cdot\sigma_2)\tau_1\cdot\tau_2[\boldsymbol{k}^{\dagger 2}\delta(\boldsymbol{r}_1 - \boldsymbol{r}_2) + \delta(\boldsymbol{r}_1 - \boldsymbol{r}_2)\boldsymbol{k}^2] \\ & + (v_{20} + v_{21}\sigma_1\cdot\sigma_2)\tau_1\cdot\tau_2[\boldsymbol{k}^\dagger\cdot\delta(\boldsymbol{r}_1 - \boldsymbol{r}_2)\boldsymbol{k}] \\ & + v_4(\sigma_1 + \sigma_2)\tau_1\cdot\tau_2\boldsymbol{k}^\dagger\times\boldsymbol{k}, \end{aligned} \tag{11}$$

where $\boldsymbol{k} = (\overrightarrow{\nabla}_1 - \overrightarrow{\nabla}_2)/2i$ and $\boldsymbol{k}^\dagger = -(\overleftarrow{\nabla}_1 - \overleftarrow{\nabla}_2)/2i$. The coefficients in Eq. (11) can be found in the Appendix of Ref. [16] or in Ref [17].

Assuming the proton–neutron particle–particle (p–p) effective interaction is local, similar to the p–h channel, we can write $\bar{v}_{\rm pp}$ as

$$\bar{v}_{\rm pp}(12;1'2') = V_{\rm pp}(\boldsymbol{r}_1\sigma_1\tau_1, \boldsymbol{r}_2\sigma_2\tau_2)\delta(\boldsymbol{r}'_1 - \boldsymbol{r}_1)\delta_{\sigma'_1,\sigma_1}\delta_{\tau'_1,\tau_1}\delta(\boldsymbol{r}'_2 - \boldsymbol{r}_2)\delta_{\sigma'_2,\sigma_2}\delta_{\tau'_2,\tau_2}. \tag{12}$$

The residual interaction in the p–p channel $V_{\rm pp}$ could be derived from the proton–neutron pairing EDF. However, this is not yet well established. What we need in our framework is an interaction between the proton–neutron particle–particle (p–p) and hole–hole (h–h) pairs. In the present calculation, we consider the p–p (h–h) interaction between the $T = 0$, $S = 1$ pair only:

$$V_{\rm pp}(\boldsymbol{r}_1\sigma_1\tau_1, \boldsymbol{r}_2\sigma_2\tau_2) = \frac{1 + P_\sigma}{2}\frac{1 - P_\tau}{2}v(\boldsymbol{r}_1)\delta(\boldsymbol{r}_1 - \boldsymbol{r}_2) \tag{13}$$

and take $v(\boldsymbol{r}) = v_0$ as a constant for simplicity. Here, P_τ denotes the isospin exchange operator.

The GT$^\pm$ transition strengths to the state i with angular momentum $K\,(K = 0, \pm1)$ are calculated as

$$B({\rm GT}^\pm; i) = \frac{g_A^2}{4\pi}|\langle i|\hat{F}^\pm_K|0\rangle|^2, \tag{14}$$

$$\langle i|\hat{F}^\pm_K|0\rangle = \sum_{\alpha\beta} X^i_{\alpha\beta}\langle\alpha\beta|\hat{F}^\pm_K|{\rm HFB}\rangle - Y^i_{\alpha\beta}\langle\alpha\beta|\hat{F}^\mp_K|{\rm HFB}\rangle \tag{15}$$

under the quasiboson approximation. The HFB vacuum is denoted as $|{\rm HFB}\rangle$, and $|\alpha\beta\rangle = \hat{a}^\dagger_{\alpha,\nu}\hat{a}^\dagger_{\beta,\pi}|{\rm HFB}\rangle$ is a 2qp excited state. The GT$^\pm$ operators are given by

$$\hat{F}^+_K = \sum_{\sigma\sigma'}\int d\boldsymbol{r}\hat{\psi}^\dagger_\nu(\boldsymbol{r}\sigma')\langle\sigma'|\sigma_K|\sigma\rangle\hat{\psi}_\pi(\boldsymbol{r}\sigma), \tag{16}$$

$$\hat{F}^-_K = \sum_{\sigma\sigma'}\int d\boldsymbol{r}\hat{\psi}^\dagger_\pi(\boldsymbol{r}\sigma')\langle\sigma'|\sigma_K|\sigma\rangle\hat{\psi}_\nu(\boldsymbol{r}\sigma). \tag{17}$$

The transition-strength distributions are presented as functions of the excitation energy E^* with respect to the ground state of the odd–odd daughter nucleus

$$R^\pm(E^*) = \sum_K\sum_i \frac{\gamma/2}{\pi}\frac{|\langle i|\hat{F}^\pm_K|0\rangle|^2}{[E^* - (\omega_i - E_0)]^2 + \gamma^2/4} \tag{18}$$

by following the procedure given in the literature [6–8,18–20] to compare our results with those in the preceding papers. The smearing width γ is introduced to make the strength distributions easier to

Table 1. Ground-state properties of Zr isotopes obtained by the deformed HFB calculation with the SkM* and mixed-type pairing ($t'_0 = -240$ MeV fm^3) interactions. Chemical potentials λ_q, deformation parameters β_2^q, average pairing gaps $\langle\Delta\rangle_q$, root-mean-square radii $\sqrt{\langle r^2\rangle_q}$ for neutrons and protons, the lowest 2qp excitation energy E_0, and Q values of β decay are listed.

	^{98}Zr	^{100}Zr	^{102}Zr	^{104}Zr	^{106}Zr	^{108}Zr	^{110}Zr	^{112}Zr
λ_ν(MeV)	−5.68	−6.91	−6.14	−5.51	−4.88	−4.57	−4.31	−3.76
λ_π(MeV)	−10.0	−10.6	−11.4	−12.2	−12.9	−13.6	−14.3	−15.0
β_2^ν	0.00	0.38	0.39	0.39	0.38	0.37	0.37	0.39
β_2^π	0.00	0.41	0.43	0.43	0.42	0.42	0.42	0.43
$\langle\Delta\rangle_\nu$ (MeV)	0.63	0.00	0.51	0.00	0.54	0.78	0.55	0.00
$\langle\Delta\rangle_\pi$ (MeV)	0.00	0.32	0.00	0.00	0.00	0.00	0.00	0.00
$\sqrt{\langle r^2\rangle_\nu}$ (fm)	4.47	4.60	4.65	4.70	4.74	4.77	4.82	4.88
$\sqrt{\langle r^2\rangle_\pi}$ (fm)	4.28	4.43	4.46	4.48	4.50	4.51	4.53	4.56
E_0 (MeV)	1.93	1.20	1.09	1.48	1.32	1.45	1.47	1.89
Q_β (MeV)	3.17	3.27	4.95	5.99	7.48	8.36	9.30	10.1

Table 2. Same as Table 1 but obtained with the SLy4 and mixed-type pairing ($t'_0 = -290$ MeV fm^3) interactions.

	^{98}Zr	^{100}Zr	^{102}Zr	^{104}Zr	^{106}Zr	^{108}Zr	^{110}Zr	^{112}Zr
λ_ν (MeV)	−5.52	−6.05	−5.41	−4.90	−4.48	−4.00	−3.53	−2.90
λ_π (MeV)	−11.1	−11.4	−12.2	−13.0	−13.9	−14.8	−15.5	−16.4
β_2^ν	0.00	0.38	0.38	0.39	0.38	0.36	0.38	0.40
β_2^π	0.00	0.40	0.41	0.43	0.42	0.41	0.42	0.44
$\langle\Delta\rangle_\nu$ (MeV)	1.04	0.60	0.70	0.71	0.72	0.54	0.65	0.00
$\langle\Delta\rangle_\pi$ (MeV)	0.00	0.62	0.53	0.27	0.00	0.33	0.00	0.00
$\sqrt{\langle r^2\rangle_\nu}$ (fm)	4.48	4.62	4.66	4.70	4.74	4.77	4.83	4.89
$\sqrt{\langle r^2\rangle_\pi}$ (fm)	4.29	4.44	4.47	4.49	4.51	4.53	4.56	4.59
E_0 (MeV)	2.69	1.48	1.41	1.42	1.59	1.69	1.83	1.74
Q_β (MeV)	3.67	4.65	6.16	7.46	8.61	9.89	10.9	12.5

read. E_0 denotes the lowest quasiparticle energy of protons and neutrons. When either or both pairing gaps vanish, we take the lowest occupied neutron and unoccupied proton states for the t_- channel. It is noted that the spin-parity of the state with E_0 is, in general, different from 1^+. The transition-strength distributions can be presented as functions of the excitation energy E_T with respect to the ground state of the mother (target) nucleus

$$R^{\pm}(E_T) = \sum_K \sum_i \frac{\gamma/2}{\pi} \frac{|\langle i|\hat{F}^{\pm}_K|0\rangle|^2}{[E_T - \{\omega_i \pm (\lambda_\nu - \lambda_\pi)\}]^2 + \gamma^2/4}. \tag{19}$$

We are going to summarize in Tables 1 and 2 the chemical potentials of protons and neutrons together with the E_0 values in the Zr isotopes under investigation. One can thus transform the excitation energy from E^* to E_T easily.

2.2. *Details of the numerical calculation*

We employ the SkM* [21] and SLy4 [22] EDFs for the mean-field Hamiltonian and the residual interaction in the p–h channel because the deformation properties were taken into account in the

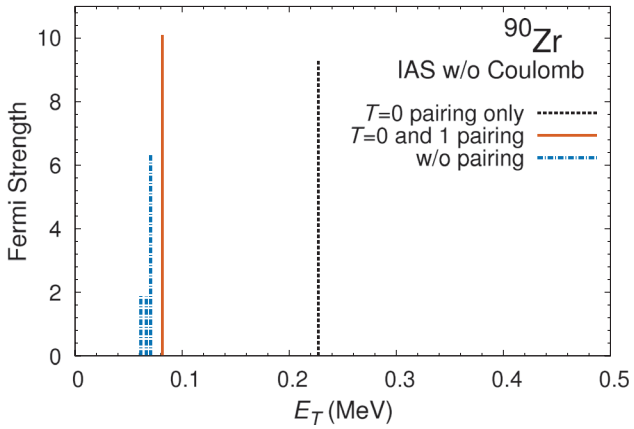

Fig. 1. Fermi-strength distributions for the t^- channel in ^{90}Zr calculated with SkM* without the Coulomb interaction as functions of the excitation energy with respect to the ground state of ^{90}Zr.

fitting procedure and we expect the evolution of deformation to be well described by SkM*, and the ground-state properties in the Zr isotopes were investigated in detail by using SLy4 in Ref. [12]. The pairing strength parameter t_0' is determined so as to approximately reproduce the experimental pairing gap of ^{120}Sn ($\Delta_{\rm exp} = 1.245$ MeV) as in Ref. [23], where the giant monopole resonance in the deformed neutron-rich Zr isotopes was investigated. The strengths $t_0' = -240$ and -290 MeV fm^3 for the mixed-type interaction ($t_3' = -18.75t_0'$) [24] lead to the neutron pairing gap $\langle\Delta_\nu\rangle = 1.20$ and 1.24 MeV in ^{120}Sn with the SkM* and SLy4 EDFs, respectively. The strength parameter v_0 for the $T = 0$ pairing interaction can be considered as a free parameter, because it dose not affect the ground-state properties, and it is active only in the dynamic level. Our procedure to determine it is to fit approximately the β-decay lifetime of ^{100}Zr ($T_{1/2}^{\rm exp} = 7.1$ s [25]). The strengths $v_0 = -395$ and -320 MeV fm^3 give the calculated β-decay half-life $T_{1/2} = 7.08$ s and 7.63 s with the SkM* and SLy4 EDFs, respectively.

Because of the assumption of the axially symmetric potential, the z-component of the qp angular momentum, Ω, is a good quantum number. Assuming time-reversal symmetry and reflection symmetry with respect to the x–y plane, we have only to solve Eq. (1) for positive Ω and positive z. We use the lattice mesh size $\Delta\rho = \Delta z = 0.6$ fm and a box boundary condition at $\rho_{\rm max} = 14.7$ fm, $z_{\rm max} = 14.4$ fm to discretize the continuum states. The differential operators are represented by use of the 13-point formula of the finite difference method. The quasiparticle energy cutoff is chosen at $E_{\rm qp,cut} = 60$ MeV and quasiparticle states up to $\Omega^\pi = 31/2^\pm$ are included.

We introduce an additional truncation for the pnQRPA calculation, in terms of the 2qp energy as $E_\alpha + E_\beta \leq 60$ MeV. This reduces the number of 2qp states to, for instance, about 30 000 for the $K^\pi = 0^+$ excitation. The number of 2qp states included in the calculation is large enough to satisfy the Ikeda sum-rule values to an accuracy of 1%. The calculation of the QRPA matrix elements in the qp basis and diagonalization of the QRPA matrix are performed on parallel computers as in Ref. [26].

As a test calculation, our method is applied to the isobaric analogue state (IAS) in ^{90}Zr. Figure 1 shows the Fermi-strength distributions for the t^- channel. When the Coulomb potential is discarded, i.e., the electron charge e is set to zero, the IAS appears at 0.23 MeV excitation energy with respect to the ground state of ^{90}Zr with the SkM* EDF and the 2qp energy cutoff described above. The transition strength to the IAS is 9.3, which is smaller than the sum-rule value of $N - Z = 10$. We find that the states at -1.35 and 1.47 MeV possess strengths of 0.36 and 0.32, respectively. When the

pairing interaction (2) is discarded further in the HFB calculation, the IAS appears at ~ 0.07 MeV, as shown in Fig. 1 by the blue dashed lines. This implies that our calculation scheme satisfies the self-consistency between the static and dynamic calculations [27,28] in the p–h channel. It is noted here that the mean energy of the IAS is given by

$$\langle E_{\rm IAS}\rangle = e^2 \int d\boldsymbol{r} \int d\boldsymbol{r}' \frac{\varrho_\pi(\boldsymbol{r})[\varrho_\nu(\boldsymbol{r}') - \varrho_\pi(\boldsymbol{r}')]}{(N-Z)|\boldsymbol{r}-\boldsymbol{r}'|} \tag{20}$$

with the sum-rule method for the separable interaction [1]. Thus, without the Coulomb potential, the excitation energy would be zero if and only if the isospin is a good quantum number [28]. The finite excitation energy of ~ 0.1 MeV obtained here is due to the numerical inaccuracy originating from the finite mesh size and the rectangular box employed for discretizing the continuum states. About 0.1 MeV differences in the calculations between HFB + pnQRPA and HF + pnRPA are due to the spurious isospin mixing in the present HFB + pnQRPA approach for $N \neq Z$ nuclei. Indeed, we obtained the IAS at 0.08 MeV, as shown in Fig. 1 by the red solid line, when we employed the mixed-type pairing interaction (2) in not only the $T = 1$ channel but also the $T = 0$ channel of the pnQRPA calculation. This result is closer to that obtained in the calculation without the pairing interactions.

As stated in the introduction, a similar calculation of the self-consistent HFB + pnQRPA for axially deformed nuclei has recently been reported [10]. They adopt the canonical-basis representation and introduce a further truncation according to the occupation probabilities of 2qp excitations. In contrast, we adopt the qp representation and truncation simply due to the 2qp energies.

3. Results and discussion

3.1. Ground-state properties

In Tables 1 and 2, we summarize the ground-state properties of the Zr isotopes calculated with the SkM* and SLy4 EDFs combined with the mixed-type pairing interaction. The ground state of ^{98}Zr is spherical, and we see a sudden onset of deformation in the Zr isotopes with $N \geq 60$. Both Skyrme EDFs give similar deformations and root-mean-square radii of the ground states in the nuclei under investigation. In the present article, we investigate the GT excitation mainly in deformed nuclei. However, to see the deformation effect, we include ^{98}Zr as a reference.

The pairing properties calculated with the two EDFs seem rather different; SkM* combined with the mixed-type pairing interaction gives weaker pairing correlations. For instance, the pairing gap of neutrons in ^{100}Zr vanishes, and both neutrons and protons are unpaired in ^{104}Zr with SkM*. For ^{112}Zr, both neutrons and protons are calculated to be unpaired consistently with the SkM* and SLy4 EDFs. The deformed shell gap of neutrons formed by between [402]5/2 and [541]1/2 orbitals and of protons formed by between [431]1/2 and [422]5/2 orbitals are 1.39 (2.01) MeV and 1.96 (1.64) MeV, respectively, with SkM* (SLy4).

For each isotope in the tables, the neutron chemical potential is shallower and the proton chemical potential is deeper with SLy4 than with SkM*. This gives larger Q_β values of β-decay with the SLy4 EDF because the differences in E_0 are not very large. The Q_β value is given by

$$\begin{aligned} Q_\beta &= M(A,Z) - M(A,Z+1) - m_e \\ &= (m_n - m_p - m_e) + B(A,Z+1) - B(A,Z) \\ &\simeq \Delta M_{n-\rm H} + \lambda_\nu - \lambda_\pi - E_0 \end{aligned} \tag{21}$$

under the independent quasiparticle approximation. Here $\Delta M_{n-\mathrm{H}} = 0.782\,27$ MeV is the mass difference between a neutron and a hydrogen atom. Note that Q_β is given by $\Delta M_{n-\mathrm{H}} - \min(\varepsilon_\pi^{\mathrm{unocc.}} - \varepsilon_\nu^{\mathrm{occ.}})$ in terms of the single-particle energies for unpaired systems if we choose E_0 as described above.

3.2. GT giant resonance

Figure 2 shows the strength distributions associated with the GT^- operator (17) without the $T = 0$ pairing in the Zr isotopes as functions of the excitation energy with respect to the daughter nuclei. We also show in this figure the contribution of the $K = 0$ and 1 components to the total strength. As we will discuss in Sect. 3.3, we see a tiny amount of energy change due to $T = 0$ pairing for the GT giant resonance (GR). We need to multiply the strengths shown in the figure by $g_A^2/4\pi$ or $(g_A^2)_{\mathrm{eff}}/4\pi$ including the quenching effect to obtain the $B(\mathrm{GT}^-)$ values in Eq. (14).

To quantify the excitation energy of the GR, we introduce the centroid energy, which is frequently used in the experimental analysis, defined by

$$E_c = \frac{m_1}{m_0}, \tag{22}$$

where m_k is a kth moment of the transition-strength distribution in an energy interval of $[E_a, E_b]$ MeV,

$$m_k \equiv \sum_K \sum_{E_a < E_i^* < E_b} E_i^{*k} |\langle i | \hat{F}_K^{\pm} | 0 \rangle|^2, \tag{23}$$

with $E_i^* = \omega_i - E_0$.

In Fig. 3(a), we show the centroid energies of the GTGR and the isobaric analogue resonance (IAR). We take the energy interval to evaluate the centroid energy of IAR as $E_a = 0$ and $E_b = 40$ MeV. For evaluation of the centroid energy of the GTGR, we take $E_a = 15$ and $E_b = 30$ MeV.

The centroid energies obtained with the SkM* and SLy4 EDFs of the GTGR are similar to each other. The properties of a GR are linked to the nuclear matter properties. In nuclear matter, the interaction strength in the GT channel is sensitive to the Landau–Migdal (LM) parameter g_0' [29]. The SkM* and SLy4 EDFs give similar values of g_0': 0.94 and 0.90, respectively. Thus, the collectivity of the calculated GTGR may be similar. These values of g_0' are large and comparable with $g_0' = 0.93$ of the SGII interaction [29], which is designed to describe spin–isospin excitations. Note that the g_0' values here were obtained in Ref. [18].

We now discuss the deformation effects. In the spherical ^{98}Zr nucleus, the centroid energy of the GTGR is about 20 MeV, and it appears as a narrow peak. Besides the GTGR, we see a low-energy resonance structure in the energy region of 5–15 MeV. When the system gets deformed, the strengths of both the GTGR and the low-energy resonance are fragmented. The deformation splitting between the $K = 0$ and 1 states of the GTGR is at most 1 MeV. So, the splitting effect is washed out by the smearing width γ. This is consistent with the finding in Ref. [19], where the schematic residual interaction was employed. The spreading effect $\Gamma^\downarrow$ not taken in the present calculation may be larger than 1 MeV so that it is difficult to observe the deformation splitting of the GTGR experimentally.

On increasing the neutron number, the centroid energy of the GTGR monotonically increases. This characteristic feature of increase in the excitation energy as a function of the neutron (mass) number is also found in Ref. [20]. In ^{112}Zr, the centroid energy reaches about 25 MeV. We also find a monotonic increase in the centroid energy of the IAR in the deformed systems. Seen is a general feature that the energies of the IAR calculated with SLy4 are higher than those calculated with SkM*.

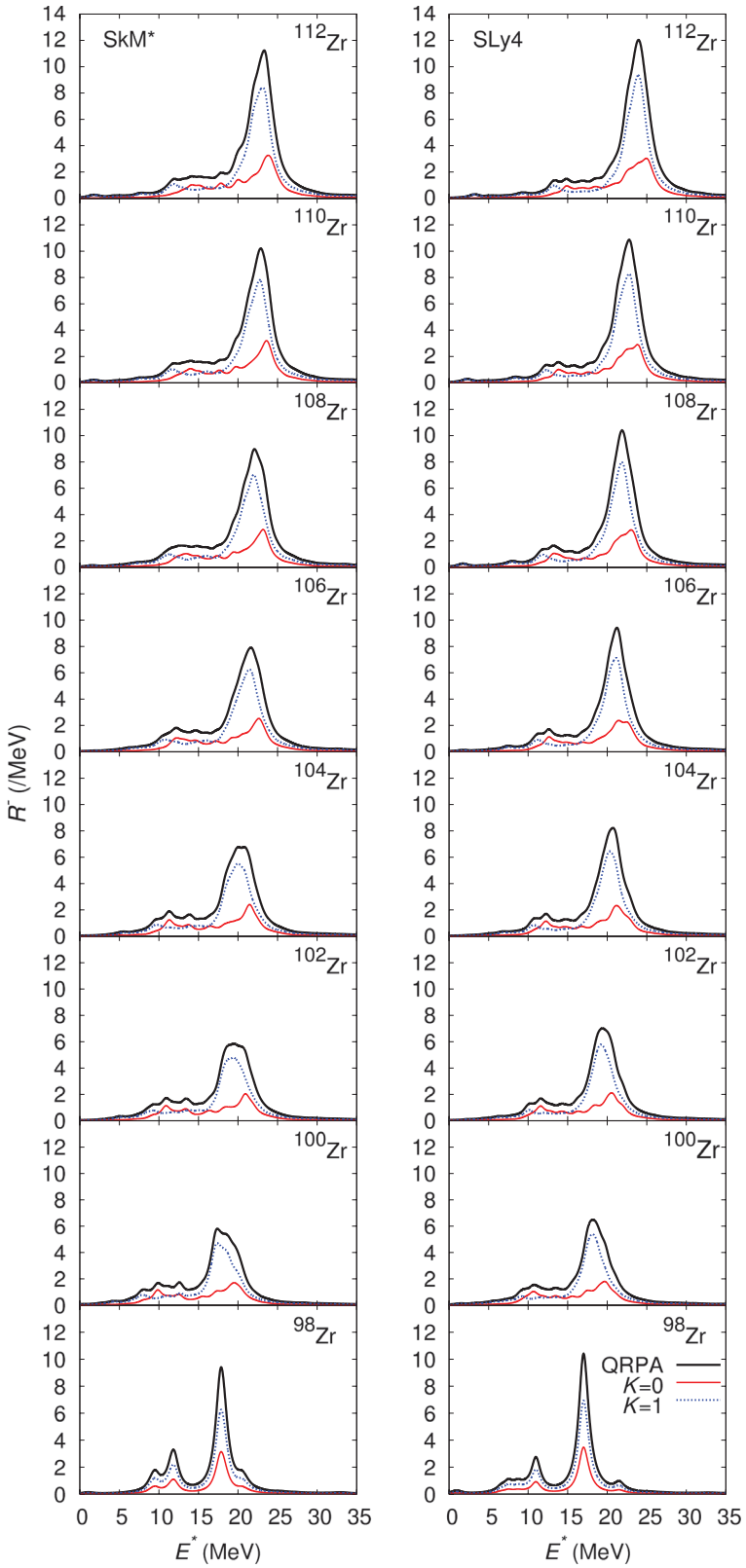

Fig. 2. Strength distributions $R^{-}(E^{*})$ as functions of the excitation energy of daughter nuclei. The SkM* (left) and SLy4 (right) EDFs combined with the mixed-type pairing interaction are employed for the calculation. The smearing width γ is set to 1 MeV.

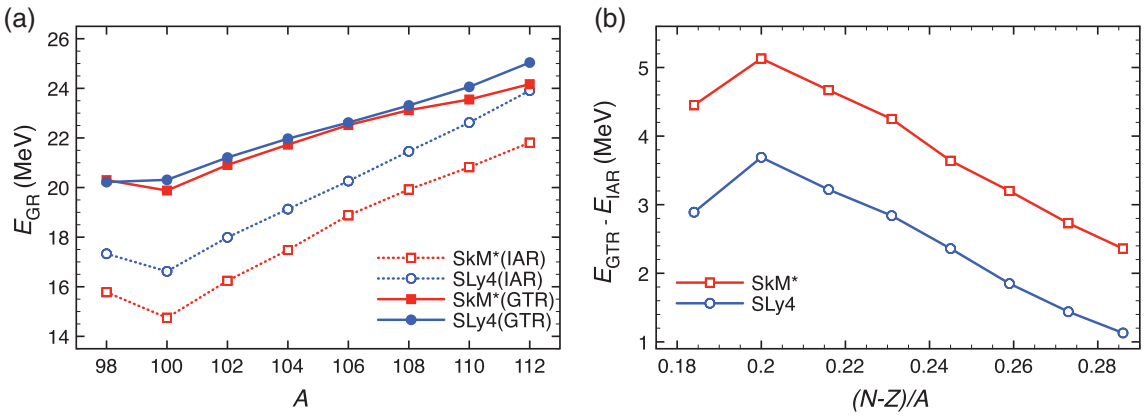

Fig. 3. (a): Centroid energies of the Gamow–Teller (GTR) and isobaric analogue (IAR) resonances in the Zr isotopes as functions of the mass number calculated with the SkM* and SLy4 EDFs. (b): Energy differences of the GTR and IAR in the Zr isotopes as functions of the relative neutron excess.

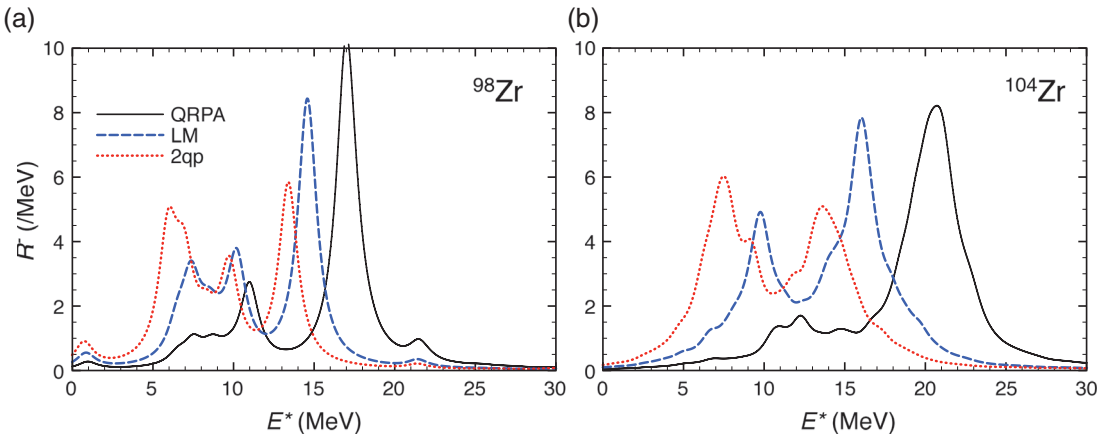

Fig. 4. Strength distributions in (a) ^{98}Zr and (b) ^{104}Zr calculated by employing the SLy4 EDF with $\gamma = 1$ MeV. The QRPA strengths are compared with the results obtained in the Landau–Migdal approximation (LM) and without the residual interactions (2qp).

It is noted that there has been a discussion on the correlation between the symmetry energy and the energy of the IAR [30]. Indeed, the symmetry coefficient of SLy4 (32.00 MeV) is larger than that of SkM* (30.03 MeV).

With the sum-rule method for the separable interaction [1], the energy difference of the GTGR and IAR is given by

$$\langle E_{\rm GTR}\rangle - \langle E_{\rm IAR}\rangle = \Delta E_{ls} + 2(\tilde{\kappa}_{\sigma\tau} - \tilde{\kappa}_{\tau})\frac{N-Z}{A}, \tag{24}$$

where ΔE_{ls} is an average value of the spin-orbit splitting, and $\tilde{\kappa}_{\sigma\tau}$ and $\tilde{\kappa}_{\tau}$ are the coupling constants of the spin–isospin and isospin residual forces in the separable Hamiltonian. The result shown in Fig. 3(b) suggests that our microscopic calculation obeys this simple relation in a good approximation as long as deformed systems are considered. The slope parameters $\tilde{\kappa}_{\sigma\tau} - \tilde{\kappa}_{\tau}$ fitted for SkM* and SLy4 in the deformed Zr isotopes are -16.7 and -15.6 MeV, respectively. The slope parameters microscopically obtained here are not far from the systematic value of -14.5 MeV [31].

Figure 4 shows the strength distributions in some selected isotopes calculated with the SLy4 EDF. In deformed isotopes other than ^{104}Zr, we see similar features, discussed below. Here, we compare the

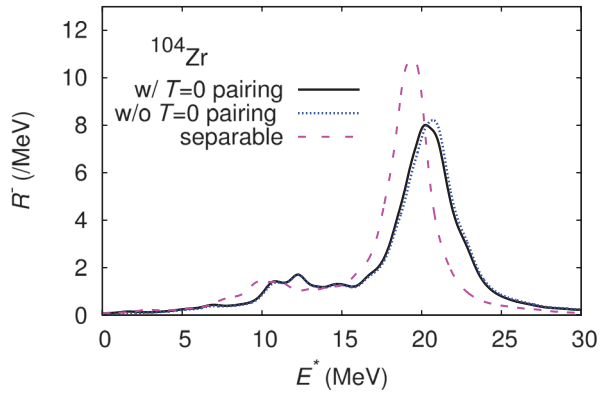

Fig. 5. Strength distributions in ^{104}Zr calculated by employing the SLy4 EDF combined with and without the $T = 0$ pairing interaction. The result in Ref. [20] employing the separable interaction is also shown.

QRPA results with those obtained in the LM approximation, and those obtained without the residual interactions. In the LM approximation, we treat the p–h residual interaction as

$$V_{\rm ph}(\boldsymbol{r}_1\sigma_1\tau_1, \boldsymbol{r}_2\sigma_2\tau_2) = N_0^{-1}\left[f_0'\tau_1\cdot\tau_2 + g_0'\sigma_1\cdot\sigma_2\tau_1\cdot\tau_2\right]\delta(\boldsymbol{r}_1 - \boldsymbol{r}_2) \tag{25}$$

instead of (11). Here, N_0 is the density of states and the LM parameters f_0', g_0' are deduced from the same Skyrme force that generates the mean field [32]. The Fermi momentum k_F appearing in the LM parameters is evaluated in the local density approximation.

In both nuclei, one of which is spherical and the other deformed, we see two prominent peaks at around 6 and 14 MeV in the unperturbed 2qp transition-strength distribution. A difference to be noticed is that the strengths are fragmented in ^{104}Zr due to deformation at the mean-field level. Associated with the repulsive p–h residual interaction, most of the strengths are absorbed by the GTGR, and the resonance peak is shifted higher in energy. The energy shift due to the RPA correlation is much larger in ^{104}Zr than in ^{98}Zr. It is pointed out that the energy and collectivity of the GTGR are changed when omitting the momentum-dependent terms in the residual interaction for the SLy5 EDF in a spherical HF-BCS + pnQRPA framework [17]. We clearly see here that the momentum dependence in the p–h residual interaction has a significant effect in generating the collectivity of the GTGR for the SkM* and SLy4 EDFs.

3.3. $T = 0$ *pairing in the GT excitation and* β*-decay rate*

The $T = 0$ pairing interaction is effective for the GT excitation in systems where the ground states have $T = 1$ pairing condensates. Both neutrons and protons are paired in ^{104}Zr with the SLy4 and mixed-type pairing EDF. Thus, we expect to see the effects of $T = 0$ pairing on the GT strength distribution in ^{104}Zr.

Figure 5 shows the strength distributions associated with the GT$^-$ operator (17) with the SLy4 EDF combined with and without the $T = 0$ pairing interaction in ^{104}Zr. We see only a tiny amount of energy change due to $T = 0$ pairing for the GTGR. The change in the centroid energy of the GTGR due to $T = 0$ pairing is 0.14 MeV. This result indicates that the GTGR is built almost entirely of p–h excitations.

In Fig. 5, we also show the result in Ref. [20], where separable forces were employed for the residual interactions. As discussed in the previous subsection, the momentum-dependent terms in the p–h residual interaction play an important role in generating the collectivity. The peak energy calculated in Ref. [20] is lower than our result by about 1.5 MeV.

Compared to the GTGR, the low-lying GT strength distribution is affected appreciably by the $T = 0$ pairing interaction due to the following mechanism showing up from the structure of the matrix elements of the pnQRPA Hamiltonian (7) and (8). The proton orbitals around the Fermi level are partially occupied due to the $T = 1$ pairing correlations. Thus, the neutrons in the hole orbitals can have a chance to interact with protons in the particle-like and hole-like orbitals through the p–h residual interaction and the $T = 0$ p–p interaction, respectively. Similarly, when the neutrons are paired, the neutrons in the particle-like and hole-like orbitals can interact with protons in the particle orbitals through the p–p and p–h residual interactions, respectively. We are considering here the t_- channel, but it also holds for the t_+ channel.

Figure 6 shows the strength distributions in the low-excitation energy region in the deformed Zr isotopes. In this figure, the smearing width γ is set to 0.1 MeV. The low-lying states are sensitive to the shell structure around the Fermi levels; however, we see some generic features: the peak position is shifted lower in energy and at the same time the transition strength increases. Note that the pairing gaps vanish in ^{104}Zr with SkM* and in ^{112}Zr with both SkM* and SLy4, and that the proton–neutron residual paring interaction does not affect the GT strength distributions in these isotopes.

In well deformed nuclei, the asymptotic quantum numbers of a single-particle orbital are approximately good quantum numbers. Though the selection rules based on the Nilsson wave functions are broken in a loosely bound system as pointed out in Ref. [33], they serve as a zeroth order guideline for understanding the structure of the excitation modes. For the GT$^-$ operator, the nonvanishing matrix elements in $N > Z$ nuclei are given as [19]

$$|\langle \pi[Nn_3\Lambda]\Omega = \Lambda \pm 1/2|t_-\sigma_{\pm 1}|\nu[Nn_3\Lambda]\Omega = \Lambda \mp 1/2\rangle| = \sqrt{2}. \tag{26}$$

In the strength distribution of ^{100}Zr calculated with SkM*, we see a prominent peak at $E^* \simeq -1$ MeV. The QRPA frequency of the lowest $K = 1$ state is $\omega = 0.33$ MeV, and the sum of backward-going amplitude squared $\sum Y^2$ is 0.49. This eigenstate is predominantly generated by a $\nu[422]3/2 \otimes \pi[422]5/2$ excitation. Note that this is an h–h type excitation because the occupation probability of a $\pi[422]5/2$ orbital is 0.78. It indicates that this mode has large transition strengths for the proton–neutron-pair creation/annihilation operators as well.

In ^{106}Zr, we see an appreciable effect of the $T = 0$ pairing interaction on the low-lying state. With SkM*, the $K^\pi = 1^+$ eigenstate at $\omega = 1.71$ MeV ($E^* = 0.39$ MeV) possessing a strength of 0.22 is mainly constructed by a $\nu[413]5/2 \otimes \pi[413]7/2$ excitation with an amplitude of $X^2 - Y^2 = 0.75$, and a $\nu[402]5/2 \otimes \pi[413]7/2$ excitation with an amplitude of 0.14. The occupation probability of a $\nu[413]5/2$ orbital is 0.12 and that of a $\nu[402]5/2$ orbital is 0.01. Thus, these 2qp excitations are a p–p type excitation, and they are sensitive to the residual pairing interaction.

In contrast, in ^{110}Zr, the effect of the $T = 0$ pairing interaction is small. The $K^\pi = 1^+$ state appearing at $\omega = 2.70$ MeV ($E^* = 1.23$ MeV) is constructed similarly in ^{106}Zr by a $\nu[413]5/2 \otimes \pi[413]7/2$ excitation with a weight of 0.38, and a $\nu[402]5/2 \otimes \pi[413]7/2$ excitation with a weight of 0.48. In ^{110}Zr, the occupation probability of a $\nu[413]5/2$ orbital is 0.78 and and that of a $\nu[402]5/2$ orbital is 0.05. Thus, the residual pairing interaction is less effective than in ^{106}Zr. With SLy4, the $K^\pi = 1^+$ state at $\omega = 4.06$ MeV ($E^* = 2.23$ MeV) possessing a strength of 0.39 is also mainly constructed by a $\nu[413]5/2 \otimes \pi[413]7/2$ excitation with a weight of 0.79, and a $\nu[402]5/2 \otimes \pi[413]7/2$ excitation with a weight of 0.17. The occupation probability of a $\nu[413]5/2$ orbital is 0.81, and that of $\nu[402]5/2$ is 0.16. Therefore, the the low-lying mode in ^{110}Zr calculated with SLy4 is dominantly a p–h type excitation and the p–p residual interaction does not play a significant role.

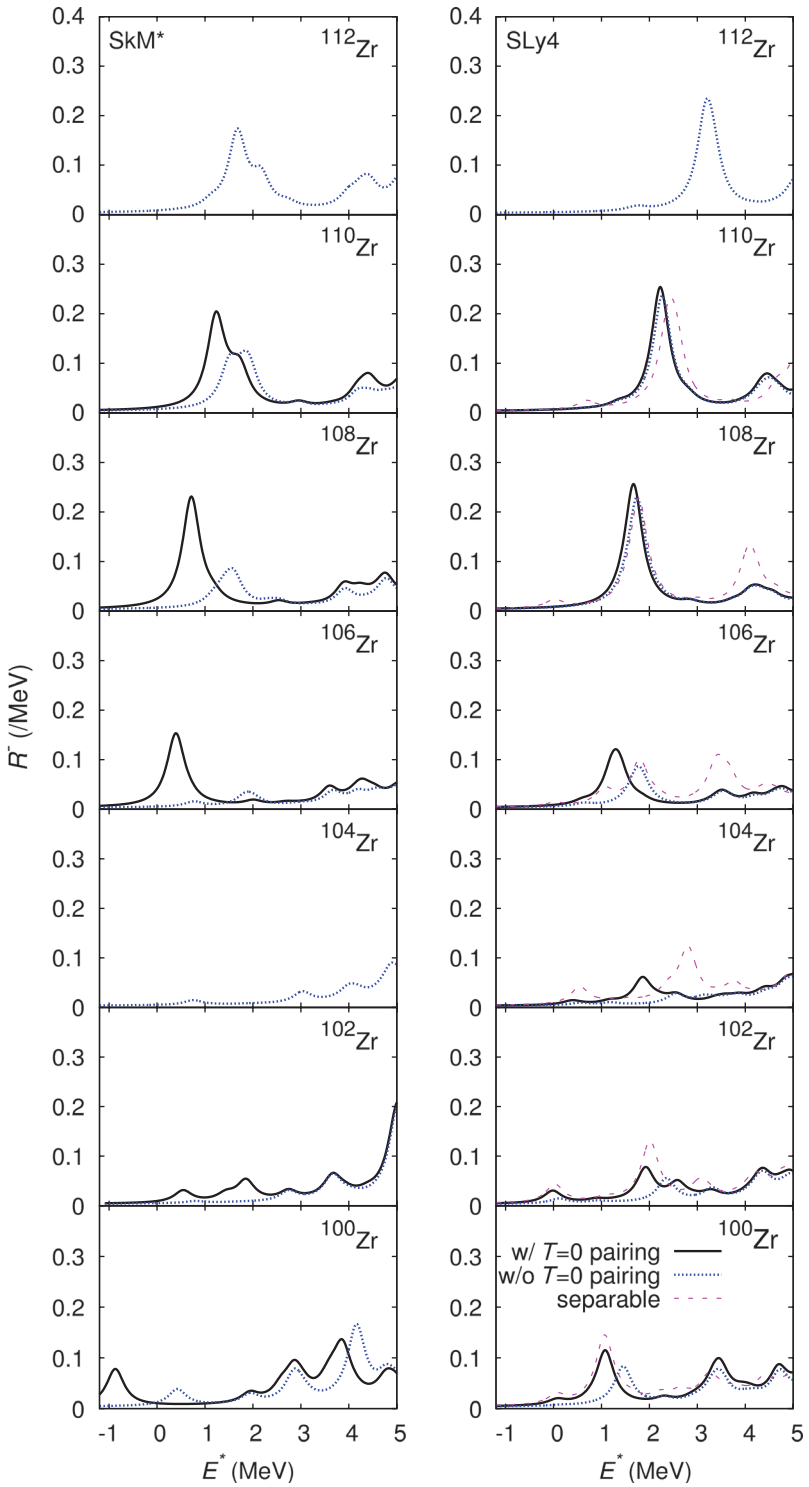

Fig. 6. Same as Fig. 5 but in the low-excitation energy region in the deformed Zr isotopes calculated with the SkM* (left) and SLy4 (right) EDFs combined with and without the $T = 0$ pairing interaction. The results in Ref. [20] are also shown. The smearing width γ is set to 0.1 MeV.

From this analysis, we come to the following conclusion: The number of 2qp excitations generating the low-lying mode is small in the Zr isotopes under consideration. The $K^\pi = 1^+$ state possessing an appreciable strength is mainly generated by a 2qp excitation satisfying the selection rule (26).

The effect of the p–p residual interaction in the low-lying mode thus depends on the location of the chemical potential, whether it is a p–h type or a p–p type excitation.

We also show the results from Ref. [20] in Fig. 6. Although the GTGR are predicted to be lower in energy in a separable approximation than by our calculations, the low-lying strength distributions are not very different. In a separable approximation, they have some small strengths in the energy region of 0–1 MeV in all the isotopes.

The low-lying GT strength distribution strongly affects the β-decay rate. Thus, we can clearly see the effect of $T = 0$ pairing in the β-decay lifetime. The β-decay half-life $T_{1/2}$ can be calculated with Fermi's golden rule as [34]

$$\frac{1}{T_{1/2}} = \frac{\lambda_\beta}{\log 2} = \frac{(g_A/g_V)^2_{\rm eff}}{D} \sum_K \sum_{E_i^* < Q_\beta} f(Z, Q_\beta - E_i^*) |\langle i|\hat{F}_K^-|0\rangle|^2, \tag{27}$$

where $D = 6163.4$ s and we set $(g_A/g_V)_{\rm eff} = 1$ rather than its actual value of 1.26 to account for the spin matrix quenching in nuclei [35]. The Fermi integral $f(Z, Q_\beta - E_i^*)$ in (27) including screening and finite-size effects is given by

$$f(Z, W_0) = \int_1^{W_0} pW(W_0 - W)^2 \lambda(Z, W) dW, \tag{28}$$

with

$$\lambda(Z, W) = 2(1+\gamma)(2pR)^{-2(1-\gamma)} e^{\pi\nu} \left| \frac{\Gamma(\gamma + i\nu)}{\Gamma(2\gamma+1)} \right|^2, \tag{29}$$

where $\gamma = \sqrt{1-(\alpha Z)^2}$, $\nu = \alpha ZW/p$, α is the fine structure constant, R is the nuclear radius. W is the total energy of the β particle, W_0 is the total energy available in $m_e c^2$ units, and $p = \sqrt{W^2 - 1}$ is the momentum in $m_e c$ units [34]. Here, the energy released in the transition from the ground state of the target nucleus to an excited state in the daughter nucleus is given approximately by [18]

$$Q_\beta - E_i^* \simeq \lambda_\nu - \lambda_\pi + \Delta M_{n-\rm H} - \omega_i. \tag{30}$$

Figure 7 shows the β-decay half-lives of the Zr isotopes thus calculated with the SkM* and SLy4 EDFs combined with and without the $T = 0$ pairing interaction. We see that the attractive $T = 0$ pairing interaction substantially shortens the β-decay half-lives.

Without the $T = 0$ pairing interaction, the half-lives calculated with SkM* are about 2–20 times longer than those with SLy4. About half of the differences are due to the smaller Q_β values calculated with SkM* than with SLy4. Thus, we need a stronger p–p interaction for SkM* to reproduce the observed half-life of ^{100}Zr. Then, the half-lives calculated with the two EDFs together with the $T = 0$ pairing interaction come closer to each other, except in ^{102,104}Zr. As mentioned in Sect. 3.1, each of the isotopes has different pairing properties depending on the Skyrme EDF employed.

In Fig. 7, we include the results from Ref. [20] together with the available experimental data [11, 25,36,37]. The recent experiment data obtained at RIKEN RIBF show the short half-lives in the ^{110}Zr region [11]. They are reproduced well by the calculation in Ref. [20], while it overestimates the half-lives of the lighter Zr isotopes. A good reproduction of the half-lives in the $A \sim 110$ region may be due to the presence of the low-lying strengths. Our calculations, in particular employing SLy4, reproduce well the observed half-lives systematically in $^{100-110}$Zr.

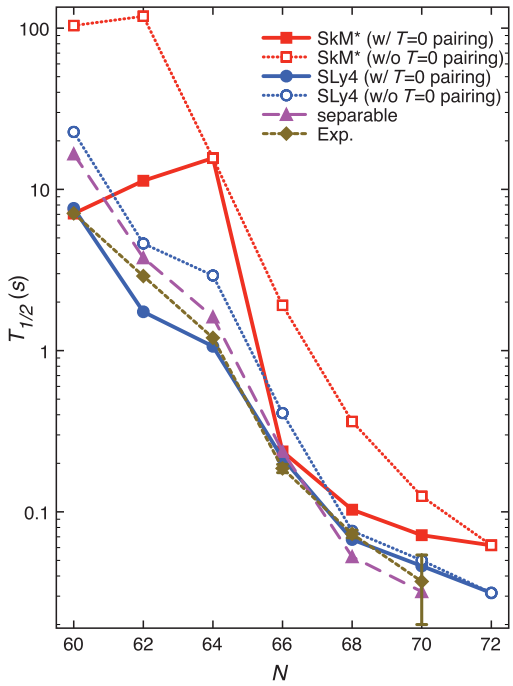

Fig. 7. Calculated β-decay half-lives of the Zr isotopes with the SkM* and SLy4 EDFs combined with and without the $T = 0$ pairing interaction. The results from Ref. [20] and experimental data [11,25,36,37] are also shown.

The low-lying GT strengths relevant to the β-decay rate are quite a delicate quantity because they emerge as a consequence of cancellation between a repulsive p–h residual interaction and an attractive $T = 0$ pairing interaction, both of which are largely uncertain in the nuclear EDF method. We need a more reliable EDF together with a proton–neutron pairing interaction that is able to describe well the spin–isospin excitations systematically in order to make further steps toward a self-consistent and systematic description of β-decay of nuclei involved in r-process nucleosynthesis. One virtue of our new framework developed in the present article is that it is suitable for a systematic calculation of the spin–isospin responses of nuclei because it is applicable to a nucleus with an arbitrary mass number, whether it is spherical or deformed, deeply bound or weakly bound, in a reasonable calculation time with the help of massively parallel computers, once the EDF and the proton–neutron pairing interaction are given. Through systematic calculations employing several parameter sets of interaction and a comparison with available experimental data or observations, we can put constraints on the spin–isospin part of the new EDF and the proton–neutron pairing interaction. Then, we can proceed to a more reliable calculation.

4. Summary

We have developed a fully self-consistent framework to calculate the spin–isospin collective modes of excitation in nuclei using the Skyrme EDF. We solve the deformed HFB equations on a grid in coordinate space. This enables us to investigate the excitation modes in nuclei off the stability line with an arbitrary mass.

Numerical applications have been performed for the Gamow–Teller excitation in deformed neutron-rich Zr isotopes. We found a small amount of fragmentation due to deformation in the GT transition-strength distribution. The momentum-dependent terms in the p–h residual interaction play

an important role in generating the collectivity. An attractive $T = 0$ pairing interaction has little influence on the energy of the GT giant resonance, while it lowers the energies and enhances the GT strengths in the low-energy region. The effect of the $T = 0$ pairing interaction in the low-lying mode depends sensitively on the location of the Fermi level of neutrons.

β-decay rates depend primarily on the Q_β value, the residual interactions in both the p–h and p–p channels, and the shell structures. The framework developed in this article self-consistently treats these key ingredients on the same footing. Once the strength of the $T = 0$ pairing interaction is determined so as to reproduce the observed β-decay half-life of ^{100}Zr, our calculation scheme produces the isotopic dependence of the half-lives up to ^{110}Zr well, as was recently observed at RIKEN RIBF.

Systematic calculations with the HFB + pnQRPA for nuclei in a whole nuclear chart help us not only to understand and predict new types of collective modes of excitation in unstable nuclei, and to provide the microscopic inputs for the astrophysical simulation, but also to shed light on the nuclear EDF of new generations.

Acknowledgements

The author thanks P. Sarriguren for providing him with the GT strength distributions for comparison. He also thanks K. Matsuyanagi, N. Van Giai, H. Z. Liang, and F. Minato for stimulating discussions. This work was supported by KAKENHI Grant Nos. 23740223 and 25287065. The numerical calculations were performed on SR16000 at the Yukawa Institute for Theoretical Physics, Kyoto University and on T2K-Tsukuba, at the Center for Computational Sciences, University of Tsukuba. Some of the results were obtained by using the K computer at the RIKEN Advanced Institute for Computational Science and by pursuing HPCI Systems Research Projects (Proposal No. hp120192).

References

[1] F. Osterfeld, Rev. Mod. Phys. **64**, 491 (1992).
[2] F. T. Baker et al., Phys. Rep. **289**, 235 (1997).
[3] K. Langanke and G. Martínez-Pinedo, Rev. Mod. Phys. **75**, 819 (2003).
[4] M. V. Stoitsov, J. Dobaczewski, W. Nazarewicz, S. Pittel, and D. J. Dean, Phys. Rev. C **68**, 054312 (2003).
[5] N. Paar, D. Vretenar, E. Khan, and G. Colò, Rep. Prog. Phys. **70**, 691 (2007).
[6] P. Sarriguren, E. Moya de Guerra, A. Escuderos, and A. C. Carrizo, Nucl. Phys. A **635**, 55 (1998).
[7] P. Sarriguren, E. Moya de Guerra, and A. Escuderos, Nucl. Phys. A **691**, 631 (2001).
[8] P. Sarriguren, Phys. Rev. C **86**, 034335 (2012).
[9] J. Dobaczewski, H. Flocard, and J. Treiner, Nucl. Phys. A **422**, 103 (1984).
[10] M. T. Mustonen and J. Engel, Phys. Rev. C **87**, 064302 (2013).
[11] S. Nishimura et al., Phys. Rev. Lett. **106**, 052502 (2011).
[12] A. Blazkiewicz, V. E. Oberacker, A. S. Umar, and M. Stoitsov, Phys. Rev. C **71**, 054321 (2005).
[13] K. Yoshida and N. V. Giai, Phys. Rev. C **78**, 064316 (2008).
[14] A. Bulgac, Preprint No. FT-194-1980 (Institute of Atomic Physics, Bucharest, 1980) [arXiv:nucl-th/9907088].
[15] R. R. Chasman, Phys. Rev. C **14**, 1935 (1976).
[16] J. Terasaki, J. Engel, M. Bender, J. Dobaczewski, W. Nazarewicz, and M. Stoitsov, Phys. Rev. C **71**, 034310 (2005).
[17] S. Fracasso and G. Colò, Phys. Rev. C **76**, 044307 (2007).
[18] J. Engel, M. Bender, J. Dobaczewski, W. Nazarewicz, and R. Surman, Phys. Rev. C **60**, 014302 (1999).
[19] P. Urkedal, X. Z. Zhang, and I. Hamamoto, Phys. Rev. C **64**, 054304 (2001).
[20] P. Sarriguren and J. Pereira, Phys. Rev. C **81**, 064314 (2010).
[21] J. Bartel, P. Quentin, M. Brack, C. Guet, and H.-B. Håkansson, Nucl. Phys. A **386**, 79 (1982).
[22] E. Chabanat, P. Bonche, P. Haensel, J. Meyer, and R. Schaeffer, Nucl. Phys. A **635**, 231 (1998).
[23] K. Yoshida, Phys. Rev. C **82**, 034324 (2010).
[24] K. Bennaceur and J. Dobaczewski, Comput. Phys. Commun. **168**, 96 (2005).

[25] B. Singh, Nucl. Data Sheets **109**, 297 (2008).
[26] K. Yoshida and T. Nakatsukasa, Phys. Rev. C **88**, 034309 (2013).
[27] C. A. Engelbrecht and R. H. Lemmer, Phys. Rev. Lett. **24**, 607 (1970).
[28] N. Auerbach, V. Bernard, and N. Van Giai, Nucl. Phys. A **337**, 143 (1980).
[29] N. Van Giai and H. Sagawa, Phys. Lett. B **106**, 379 (1981).
[30] P. Danielewicz and J. Lee, arXiv:1307.4130.
[31] K. Nakayama, A. Pio Galeão, and F. Krmpoti, Phys. Lett. B **114**, 217 (1982).
[32] M. Bender, J. Dobaczewski, J. Engel, and W. Nazarewicz, Phys. Rev. C **65**, 054322 (2002).
[33] K. Yoshida, M. Yamagami, and K. Matsuyanagi, Nucl. Phys. A **779**, 99 (2006).
[34] N. B. Gove and M. J. Martin, At. Data Nucl. Data Tables **10**, 205 (1971).
[35] A. Bohr and B. R. Mottelson, *Nuclear Structure* (Benjamin, New York, 1975), Vol. 2.
[36] D. De Frenne, Nucl. Data Sheets **110**, 1745 (2009).
[37] J. Blachot, Nucl. Data Sheets **108**, 2035 (2007).